Experimental Investigation of Turbulent Boundary Layer Response to a Synthetic Large-Scale Structure

Mitchel Lozier[1], Flint O. Thomas[2], and Stanislav Gordeyev[3]
University of Notre Dame, Notre Dame, IN 46556

The dynamic response of a zero-pressure gradient turbulent boundary layer (TBL) to an active flow control actuator was experimentally investigated. The TBL has a sufficiently low momentum thickness Reynolds number, that there is not a discernable large-scale structure in the outer region as evidenced from pre-multiplied wavenumber-frequency spectra. The periodically pulsed plasma actuator, placed inside the outer region of TBL, introduces a synthetic outer large-scale structure, and the boundary layer response to this synthetic structure at various wall-normal and streamwise locations downstream of the actuator was investigated. The evolution of near-wall residual turbulence modulated by the synthetic structure in the inner and log regions of the boundary layer was analyzed using a phase-locked analysis. The dynamic interaction of the synthetic structure and smaller-scale structures was quantified using the modulation coefficient, and a strong positive correlation in the inner and log region of the boundary layer was observed. The evolution of the synthetic large-scale structure and its modulating effect on the near-wall turbulence at several streamwise locations is described. Phase profiles at different streamwise locations were extracted and were found to be constant in the log-region, further confirming a strong coupling between the near-wall turbulent fluctuations and the synthetic large-scale structure. Overall, the large-scale structure has a modulating effect on the turbulence in the near wall region, similar to the modulation observed in canonical TBLs at higher Reynolds numbers.

Nomenclature

x = streamwise coordinate

[1] Graduate Student, Department of Aerospace and Mech. Engineering, AIAA Student Member.
[2] Professor, Department of Aerospace and Mech. Engineering, AIAA Associate Fellow.
[3] Associate Professor, Department of Aerospace and Mech. Engineering, AIAA Associate Fellow.

y = wall-normal coordinate

z = spanwise coordinate

$(\cdot)^+$ = quantity normalized by inner variables

$(\cdot)^*$ = quantity normalized by outer variables

l = hot-wire length

δ = boundary layer thickness

U_∞ = free stream velocity

u_τ = friction velocity

C_f = friction coefficient

H_S = boundary layer shape factor

Re_τ = friction velocity Reynolds number

Re_θ = displacement thickness Reynolds number

H = actuator height

W = actuator width

L = actuator length

f_s = sampling frequency

Δt = time between measurements

ν = kinematic viscosity

u = streamwise velocity

v = wall-normal velocity

U = mean velocity

u_{rms} = root-mean-square of velocity

$\tilde{u}$ = modal component of velocity

u' = fluctuating component of velocity

k = wavenumber

λ_x = streamwise wavelength

Φ_{xx} = streamwise power spectral density

f_P = actuation frequency

T_P = actuation period

φ = phase of actuation cycle

n = single actuation period length realization

t_n = time within single actuation period

$\langle\cdot\rangle_n$ = ensemble average of realizations

$\langle\cdot\rangle_\varphi$ = phase average

$\Delta u'_{rms}$ = residual turbulence

Φ = modulation coefficient

f_{SS} = small-scale frequency

f_{LS} = large-scale frequency

ΔU_{max} = maximum wake velocity deficit

u_{max} = maximum jet velocity

w = wake or jet half-width

u_φ = phase velocity

U_c = convective velocity

x_P = pseudo-spatial streamwise coordinate

I. Introduction

The large-scale structures (LSS) found in the turbulent boundary layer (TBL) and their effect on technologically relevant flow properties such as skin friction and aero-optical distortion have been investigated extensively [1] [2] [3] [4]. LSS refers in general to the coherent and energetic motions with a streamwise extent on the order of a few boundary layer thicknesses that exist in high enough Reynolds number flows ($Re_\tau > 2000$) [4]. In the outer region of the TBL the LSS take the form of spanwise-oriented vortices with most of their coherent energy concentrated around the geometric center of the log-linear region of the TBL ($y^+ = 3.9Re_\tau^{0.5}$) [5] [6]. Closer to the wall the coherent structure is associated with streamwise vortices located in the buffer region that have a typical spanwise extent on the order of the boundary layer thickness [4]. These near wall streamwise vortical structures are responsible for the production of turbulence near the wall and have a significant effect on the global boundary layer dynamics as noted in many studies [1] [4].

In canonical turbulent boundary layers, thin shear layers separating low-speed and high-speed regions, referred to as uniform momentum regions, have been observed and studied [5] [6]. These thin shear layer structures, combined with the low momentum flow underneath them, are believed to be part of a coherent structure, referred to as the "Attached Eddy" [7]. A recent investigation of adverse pressure gradient TBLs demonstrated that the local flow physics is largely dominated by an embedded shear layer associated with the inflectional instability of the outer mean velocity profile inflection point [8]. Using scaling laws developed for free shear-layers applied to the adverse pressure gradient (APG) TBL, profiles of mean velocity and turbulence quantities exhibited a collapse. The generic applicability of the embedded shear layer scaling was demonstrated by collapsing multiple APG turbulent boundary layer data sets from the AFOSR-IFP-Stanford Conference compiled by Coles and Hirst [9]. Further support for the influence of the outer shear layer structure on the near-wall TBL dynamics was recently provided by a study demonstrating that the presence of a free shear layer just outside a TBL has a significant effect on the near-wall bursting and sweep events [10].

Collectively, the results described above strongly suggest that embedded shear layers are a generic feature of all TBLs irrespective of whether the mean velocity profile is inflectional. Although more apparent in APG boundary layers with inherent inflectional mean velocity profiles, transient and non-localized inflectional instabilities could well account for the enhancement of outer large-scale boundary layer structures that has been documented in previous studies of high Reynolds number zero pressure gradient TBLs [5] [6]. These shear-layer-like structures likely play an important role in determining LSS dynamics and ultimately in the global properties of the TBL.

An intriguing aspect of the presence of shear layers in the TBL is that they are very amenable to control. The ability to independently control outer layer LSS in the TBL offers new possibilities for uncovering the underlying dynamics with particular focus on the outer – inner layer interaction. This aspect has been largely unexplored since most studies and models regarding the relationship between the small- and large-scale structures deal with natural or un-manipulated TBLs and apply various conditional-averaging techniques to study their interactions [1] [3]. Only a small number of studies thus far have investigated modifying the coherent structures directly. Some of the first devices used to modify the LSS directly were outer layer, thin flat plate manipulators, sometimes referred to as Large Eddy Breakup devices (LEBU). Studies of these plate manipulators in the boundary layer showed that they were effective in modifying or reducing near-wall turbulent structures and the skin friction or aero-optical distortion as a result [11] [12]. The most direct effect of these plates was disrupting the intermittent large-scale structures in the outer layer of

the TBL which allowed less high momentum fluid to be entrained towards the wall limiting the burst and sweep events occurring during the near-wall cycle. Later, the interaction of the vortices, generated in the thin plate's wake, with the near-wall structure was shown to be another possible mechanism contributing to the overall skin friction reduction downstream of the manipulators [13]. These results suggest that in general flat plate manipulators can be used effectively to interrupt the natural non-linear interactions that occur between large-scale structures in the outer layer and small-scale structures near the wall.

Active control devices that introduce periodic large-scale motions into the TBL are another tool that have been used to study the dynamics of the TBL in recent years. In [14] [15] [16] [17] a dynamic roughness element actuated at the wall was used to introduce a periodic traveling wave, or synthetic large-scale structure, into the near-wall and log-region of the turbulent boundary layer. It was shown that the large-scale motions created by the dynamic roughness element resulted in changes to the phase of interactions between triadically coupled modes. Further, the synthetic large-scale motions had the greatest effect on small-scale motions that were triadically coupled with the imposed large-scale, resulting in an organizing effect. Importantly, this organizing effect along with mean flow and higher-order statistics had signatures of the original periodic traveling wave a significant distance downstream of the dynamic roughness location (on the order of 10 TBL thicknesses). It was also shown that the forcing frequency could be manipulated to obtain specific streamwise length scales. These controlled length scales can be selected to excite or organize specific structure sizes related to the near-wall cycle. The results of these dynamic roughness studies have shown that the TBL is receptive to the introduction of synthetic large-scale motions which can be selectively tuned to have an organizing effect on near-wall small scale structures which persists a significant distance downstream of the location of the initial perturbation.

In another recent study [10] it was observed that large-scale vortical structures traveling outside of the boundary layer can also influence the near-wall turbulence. In the cited study, a TBL was externally forced by the unsteady pressure field generated by a free shear layer and the near-wall turbulence inside the boundary layer was found to be both amplified and modulated by the external forcing. This result shows that, like the studies of internally forced boundary layers, perturbations to the outer region can also cause changes in the amplitude and organization of structures within the near-wall region of the boundary layer.

Motivated by the studies and results described above, in the current study, active flow control is used to introduce large-scale periodic motions into the outer region of a turbulent boundary layer through an active, plasma-based, thin

flat plate actuator. The synthetically imposed outer structure is a key in this study since it provides a convenient external phase reference for quantifying the outer-inner layer interaction in the TBL. The Reynolds number of the studied turbulent boundary layer is low enough that there are no naturally occurring energetic coherent large-scale structures present in the outer region. Instead, the actuator is used to introduce a synthetic large-scale periodic structure at different wall-normal locations and forcing frequencies, which determines the streamwise scale of the synthetic structure. The presented study characterizes the effect of introducing the plasma actuator into the TBL and explores the interaction between the synthetic large-scale structure, introduced by the actuator, and the naturally occurring near-wall turbulence.

II. Experimental Set-Up

The experiments in this study were performed in one of the low-turbulence, subsonic, in-draft wind tunnels located at the Hessert Laboratory for Aerospace Research at the University of Notre
Dame. The wind tunnel has an inlet contraction ratio of 6:1. A series of turbulence-management screens at the front of the inlet give rise to tunnel freestream turbulence levels of less than 0.1% (0.06% for frequencies above 10 Hz). Experiments are performed in a test section of 0.610 m square cross section and 1.82 m length.

The experimental set-up is shown schematically in Figure 1. For this study, a 2-meter-long by 0.6-meter-wide boundary layer development plate was installed along the center height of the tunnel test section. The boundary layer development plate had a sandpaper distributed roughness element attached to the leading edge of the plate; the leading edge was shaped into a semicircular profile. A constant temperature anemometer (CTA) with a single boundary layer hot-wire probe (Dantec 55P15) with diameter $5\ \mu m$ and length $l = 1.5\ mm$ (corresponding to $l^+ = 30$) was used to collect time-series of the streamwise velocity component. For this hot-wire length, the measured turbulence intensity near the wall, and specifically at its peak value, is expected to be slightly attenuated, as described by [18]. A computer controlled traversing stage was inserted through the top wall of the tunnel along the midpoint of the tunnel span to allow the hot-wire probe to traverse the test section in the wall-normal (y) direction and make time-resolved velocity measurements inside the boundary layer. The minimum step size of the traverse system was $0.00625\ mm$ ($\Delta y^+ = 0.125$).

A plasma actuator device, as described below, was attached to the top side of the boundary layer development plate at a fixed streamwise location of $140\ cm$ from the leading edge of the boundary layer development plate. The

streamwise position of the hot-wire probe traverse system is adjustable so the probe was positioned at four x-locations as measured downstream of the plasma actuator's trailing edge, to measure the time-resolved TBL response at these x-locations. The locations selected for this study were 51 mm, 102 mm, 170 mm, and 272 mm, which correspond to 1.5δ, 3δ, 5δ, and 8δ, respectively, based on the experimentally measured boundary layer thickness, δ, near the actuator trailing edge.

A set of representative canonical turbulent boundary layer characteristics were measured at the downstream location of $x = 3\delta$ using the hot-wire probe. These parameters are summarized in Table 1 for reference. The skin friction velocity u_τ was determined using the Clauser method. In all the experiments described in this study, the wind tunnel free stream velocity was 7 m/s and was measured to be within ±1% of the expected free stream velocity before each test.

Table 1. Canonical turbulent boundary layer parameters at $x = 3\delta$

δ	U_∞	u_τ	C_f	H_s	Re_θ	Re_τ
33.2 mm	6.95 m/s	0.304 m/s	0.0039	1.37	1,770	690

As shown in Figure 1, a plasma-based Active Large-Scale Structure Actuator (ALSSA) device was used in this study to introduce periodic plasma–induced forcing in the outer layer of the boundary layer. The plasma actuator was supported above the boundary layer development plate by vertical NACA0010 airfoils on both sides which were 4 mm thick, and which were made at heights, *H*, between $H = 10\ and\ 21\ mm$ ($0.3\delta\ and\ 0.6\delta$). In this manner, large-scale motions generated by the actuator, referred to as the synthetic LSS, could be introduced into the TBL at different distances away from the wall. The plasma actuator was $W = 25\ cm$ (8δ) wide in the spanwise direction and $L = 32\ mm$ ($< 1\ \delta$) long in the streamwise direction. Due to the finite spanwise width of the actuator plate and the presence of airfoil supports underneath, there are significant three-dimensional motions within 30 mm of either end of the plate at the furthest downstream measurement location as described in more detail later. The actuator plate was made of a 2 mm thick sheet of Ultem dielectric polymer. An upper surface electrode of 0.05 mm thick copper foil tape was located 15 mm from the plate leading edge and was 4 mm in length and 22 cm in width. On the lower surface a second copper foil electrode was located 15 mm from the leading edge in line with the top electrode and was 12 mm in length and 22 cm in width. The corners of the electrodes were rounded, and they were mounted in alignment to reduce extraneous regions of plasma generation and regions of highly concentrated plasma. The leading edge of the

actuator plate was rounded, and the last 10 mm of the trailing edge were linearly tapered to a half-angle of 10° to eliminate the separation region downstream of the trailing edge of the plate.

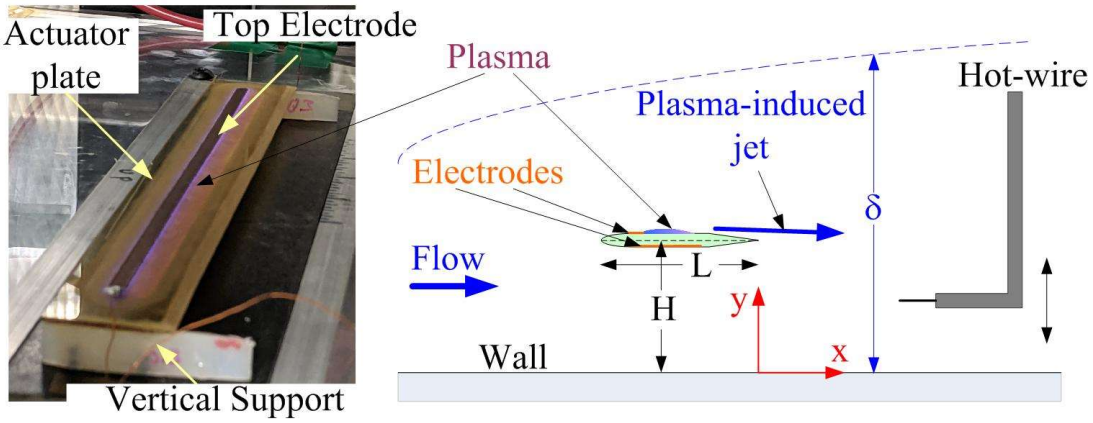

Figure 1. Schematic of experimental set-up with picture of plasma based ALSSA device in use.

The alternating current dielectric barrier discharge (AC-DBD) plasma formed on the actuator was produced using a high voltage AC source which consisted of a function generator, power amplifiers and a transformer [19]. The 0.05 mm thick copper electrodes placed on the top and bottom of the actuator were connected to the high voltage AC source which provided a 40kV peak-to-peak sinusoidal waveform excitation to the electrodes at a frequency of 4 kHz. The peak-to-peak voltage was maintained within $\pm 5\%$ of expected excitation voltage during experiments. It has been observed [20] that high relative humidity can decrease the body force produced by the actuator. This is noteworthy when discussing experimental results because the relative humidity in the laboratory which feeds the in-draft wind tunnel fluctuates between seasons. As shown in Figure 1, the intended plasma jet was formed on the top surface of the actuator plate above the exposed portion of the lower surface electrode. At the 4 kHz actuation frequency, the plasma actuator operates in a quasi-steady mode, essentially creating a spanwise-uniform steady wall jet in the streamwise direction [19]. To introduce periodic forcing, the sinusoidal waveform was modulated by a square wave with a fifty percent duty cycle oscillating at the desired forcing frequency.

A pitot probe was also inserted into the test section upstream of the plasma actuator through the side wall of the tunnel to determine the free stream velocity of the tunnel to calibrate the hot-wire probe. Hot-wire voltages, pitot probe pressure transducer voltages and the output of the function generator to the ALSSA device were digitally recorded simultaneously in every experiment. The data was sampled at f_s = 30 kHz which corresponds to $\Delta t^+ = (1/f_s)u_\tau^2/\nu =$

0.2 for a total period of at least 90 seconds, or about 15,000 δ/U_∞ in each test. With this sampling frequency and sampling time there should be no additional loss of turbulence information, compounding the spatial averaging effect of the hot-wire, as described in [18].

III. Data Reduction

The hot-wire was calibrated before and after each experiment, using standard methods [21], and the anemometer voltages were converted into velocities using a linear interpolation between the two calibrations to account for any drift in laboratory temperature over the course of the experiment. The maximum ambient temperature drift over the course of any experiment was recorded to be $0.2\ °C$ and the maximum ambient pressure drift over any one experiment was $2\ mbar$. The velocity time series were digitally band-stop filtered between 3.8-4.2 kHz to eliminate electronic noise associated with the high voltage AC source supplying the actuator. After the hot-wire voltages were converted and filtered, the time mean, U, and root mean square (RMS) of the velocity, u_{rms} , were calculated at every wall-normal y-location using standard methods. Since the actuator introduced periodic forcing into the flow, it is convenient and necessary to phase-lock the results to the periodic forcing frequency to separate the synthetic large-scale motions from the small-scale turbulent response [10].

To implement phase-locking, a triple phase-locked Reynolds decomposition of the velocity was considered, as shown in Equation 1 where u is the instantaneous velocity, U is the time mean component of velocity, $\tilde{u}$ is a phase dependent or modal velocity component, u' is a residual fluctuating turbulent component, φ is the phase, defined by the relationship in Equation 2, where n is the number of realizations.

$$u(y,t) = U(y) + \tilde{u}(y,\varphi) + u'(y,\varphi,n) \tag{1}$$

$$\varphi = \left(\frac{t_n}{T_p} - n\right) 2\pi \tag{2}$$

The n realizations are single forcing period ($T_p = 1/f_p$) length velocity time series extracted from the overall time series that each begin when the plasma is turned on in the repetition cycle. In Equation 2, t_n is a time in the n^{th} realization, which is related to the phase angle, φ, by the period of the repetition cycle. The signal produced by the function generator was used to ensure that the data was phase locked with the repetition cycle of the plasma. These n realizations of velocity time series are then ensemble averaged to find the modal component of velocity as a function

of the phase angle. In the presented experiments, $n = 7200$, ensuring a proper convergence of the ensemble averaged results. The fluctuating component of the velocity u' that remains after removing the modal component of velocity from each realization was used to quantify an ensemble-averaged root-mean-square of the residual turbulence shown in Equation 3.

$$\Delta u'_{rms} = (\langle [u'(y,\varphi,n)]^2 \rangle_n)^{\frac{1}{2}} \tag{3}$$

Here the square brackets denote ensemble averaging over all realizations. Later we will refer to this quantity as a residual turbulence level. The phase-averaged mean can be removed from the residual turbulence level to define a local change in residual turbulence. A so called Φ-coefficient, which was introduced in [9], is used to quantify the modulating effect of the large-scale motions on small-scale motions and is shown in Equation 4. This modulation coefficient correlates changes in the modal velocity, which represents large-scale motions, to those in the residual turbulence, which represents small-scale motions. Higher modulation coefficient values indicate the induced large-scale perturbation and phase-locked small-scale response are in phase.

$$\Phi(y) = \frac{\langle \tilde{u}(y,\varphi) \Delta u'_{rms}(y,\varphi) \rangle_\varphi}{\sqrt{\langle \tilde{u}(y,\varphi)^2 \rangle_\varphi} \sqrt{\langle \Delta u'_{rms}(y,\varphi)^2 \rangle_\varphi}} \tag{4}$$

IV. Actuator Optimization

There were multiple characteristics of the actuator design and operation that had to be tested and optimized before the final configuration of the actuator was chosen. The first of these characteristics was the spanwise width and streamwise length of the physical actuator plate. In preliminary tests it was found that the wake produced by the plate was a dominant feature of the flow downstream of the actuator [22]. To increase the strength of the plasma forcing relative to the plate's wake and the natural TBL structure, the streamwise length of the plate was reduced to its minimum length for safe operation. There should be approximately $5\ mm$ of dielectric per $10kV$ excitation voltage separating the electrodes as measured from the electrode's edge around the edges of the plate to prevent arcing at the voltage used in this experiment [19]. With this constraint, the final streamwise length of the actuator was set to $L = 32\ mm$. As discussed above, the goal of this actuator is to introduce spanwise-uniform, two-dimensional vortical structures into the boundary layer. The dielectric material used in the actuator plate does not have the stiffness required

to easily span the entire tunnel width without warping or vibrating excessively, so airfoil supports were used to anchor a finite width actuator plate to the wall. The finite width of the actuator plate and airfoil supports below the actuator plate introduced three-dimensional motions around the ends of the plate. The spanwise extent of the natural LSS in the TBL are on the order of the boundary layer thickness and as such the actuator should be able to introduce two-dimensional motions that are several times larger than the spanwise extent of the natural LSS to ensure its effectiveness when compared to natural LSS. To investigate the three-dimensional end effects of the plate, the actuator was placed on a traversing stage that could be moved in the spanwise z-direction, while the fixed hot-wire measured the spanwise variation in flow downstream of the actuator. Figure 2 shows the reconstructed mean velocity and RMS velocity field of the wake behind one of the airfoils ($z/\delta = 1.5$) supports attached to the end of the actuator plate. Profiles were taken at a wall-normal distance of $y^+ = 100$ and extend from the center of the plate ($z/\delta = 0$) to at least one boundary layer thickness past the end of the plate at each measurement location. The profiles were interpolated to create a reconstruction of the entire downstream field.

In Figure 2(a), the normalized mean velocity field shows that the deficit created by the plate is spreading downstream of the airfoil support out to approximately one boundary layer thickness at the farthest downstream point of $x = 8\delta$. In only this initial portion of the experiment was the actuator plate $W = 3\delta$ wide making the location of the airfoil support $z = 1.5\delta$ as seen in Figure 2. The RMS velocity, Figure 2(b), shows a similar spreading behavior. Assuming that the plate is symmetrical about its center and knowing that at least one boundary layer thickness from either side of the plate will have induced three-dimensional motions, the final spanwise width of the plate was chosen to be $W = 8\delta$. This actuator width will result in at least a 5δ wide region of approximately two-dimensional, spanwise uniform, motion centered around the midpoint of the actuator plate.

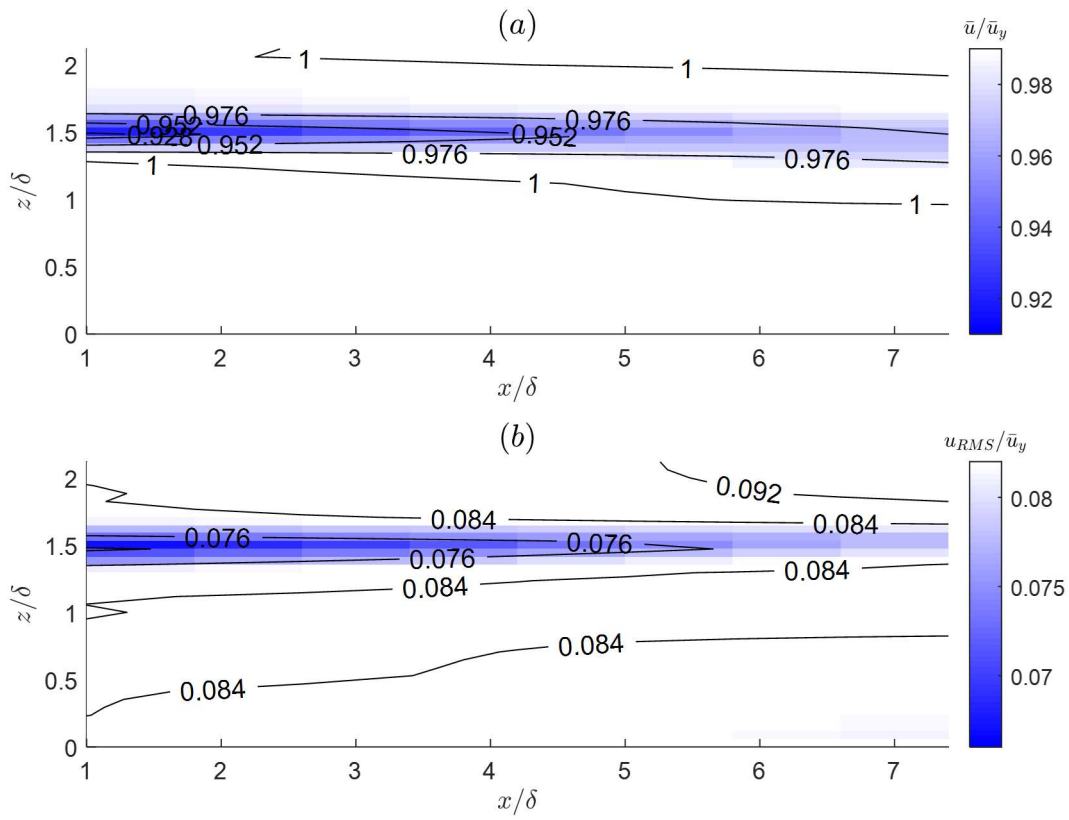

Figure 2. Spanwise-streamwise reconstruction of iso-contours of (a) mean velocity and (b) RMS velocity behind airfoil support normalized by local mean velocity. $y^+ = 100, \mathrm{H} = 0.3\delta$.

Along with the plate dimensions, the wall-normal location of the plate is an important parameter of the experiment. Parametric studies of the effect of the wall-normal actuator location, H, were conducted and discussed in a previous study [22] to investigate which wall-normal locations result in the strongest modulating effect in the near-wall region. Two wall-normal positions of $H = 0.3\delta$ and 0.6δ ($H^+ = 200$ and 400) were selected for comparison. The wall-normal position of $H = 0.6\delta$ was chosen for comparison based on the results of flat plate manipulator studies [12] which showed this was an effective wall-normal location for an actuator to mitigate existing outer layer structures. The second wall normal position of $H = 0.3\delta$ is near the upper limit of the log-linear region, as measured from the canonical TBL mean velocity profile, (see Figure 4), which is closer to the location of natural canonical spanwise oriented large-scale structures. It is also far enough from the wall to limit the unintended secondary effect of significantly accelerating the flow between the plate and the wall. As shown in the study mentioned above, there was a 20 percent reduction in turbulence intensity near the wall which is directly attributed to large-scale modulation of the residual turbulence when the plate was at the closest wall-normal position compared to the farthest. There was

also a negative shift in the skewness which is attributed to a change in the dynamics of the non-linear interactions near the wall. The phase-locking or reorganizing effect of the actuator as measured by the modulation function Φ did not change significantly between the different wall normal locations. Overall, the actuator showed the capability to modulate and phase-lock near-wall turbulence at both locations, but when it was closer to the wall the interactions between the LSS, and near-wall structures were stronger. For this reason, the current study is focused only on the wall normal location $H = 0.3\delta$ ($H^+ = 200$).

Another key parameter of the actuator design, which was expected to have a significant effect on phase-locking, was the plasma forcing frequency. The main objective of the plasma forcing is to introduce a synthetic large-scale structure of a given frequency and modify the near-wall structures to study the outer-inner interaction mechanism. The canonical boundary layer flow has two key characteristic frequencies. One is associated with the typical bursting frequency of the small-scale turbulence near the wall. In [23] this small-scale frequency, f_{SS} was determined to be approximately $f_{SS}^+ = f_{ss}\nu/u_\tau^2 = 0.011$, which would correspond to a frequency of $f_{SS} = 72$ Hz in the current experiment. The other frequency, f_{LS}, is associated with the size of naturally occurring large-scale structures. The streamwise wavelength of coherent large-scale motions in a canonical boundary layer was estimated to be $\lambda_x = 3 - 6\delta$ based on the measurements of higher Reynolds TBLs by Hutchins and Marusic [3], making the range of large-scale frequencies $f_{LS} = U_\infty/\lambda_x = 34$ – 68 Hz for the current experiment. This results in an outer scaled range of the large-scale frequencies of $f_{LS}^* = f_{Ls}\delta/U_\infty = 0.16 - 0.32$.

To investigate which frequencies will result in the strongest modulation effect near the wall, the hot-wire probe was placed in the near wall region at $y^+ = 20$ and the frequency of the plasma forcing was varied from $20 - 200\ Hz$. From instantaneous velocity data, the modal velocity and residual turbulence were calculated, and the modulation coefficient Φ (Eqn. 4) was computed for each frequency. Figure 3(a) presents the values of the modulation coefficient for different forcing frequencies at two different streamwise locations of x/δ = 3 and 8. There is a clear band of frequencies around 80-100 Hz where there is the strongest correlation between large synthetic scale, introduced by the plasma actuator, and small scales near the wall across all streamwise locations. The results of the forcing frequency experiments were normalized by the local inner and outer units and are shown in Figure 3. Closer to the actuation plate ($x = 3\delta, 5\delta$), the inner scaled peak in modulation matches the expected near wall frequency, which is around $f^+ = f\nu/u_\tau^2 = 0.01 - 0.02$ [23], Figure 3(b). Conversely farther downstream from the plate ($x = 5\delta, 8\delta$), the outer scaled peak in modulation matches the expected outer layer frequency of $f^* = f\delta/U_\infty = 0.25$, Figure 3(a). This

presents an interesting observation that immediately downstream of the actuator plate, the response of the near-wall region is most receptive to perturbations on the order of the natural near-wall structures. However, farther downstream, the near-wall region is becoming receptive or rather adjusting to the presence of the outer scaled synthetic periodic large-scale motions. For this reason, the forcing frequency was chosen to be $f_P = 80\,Hz$ ($f_P^+ = 0.012, f_P^* = 0.39$). This forcing frequency corresponds to a synthetic structure of $\lambda_x = 2.5\delta$.

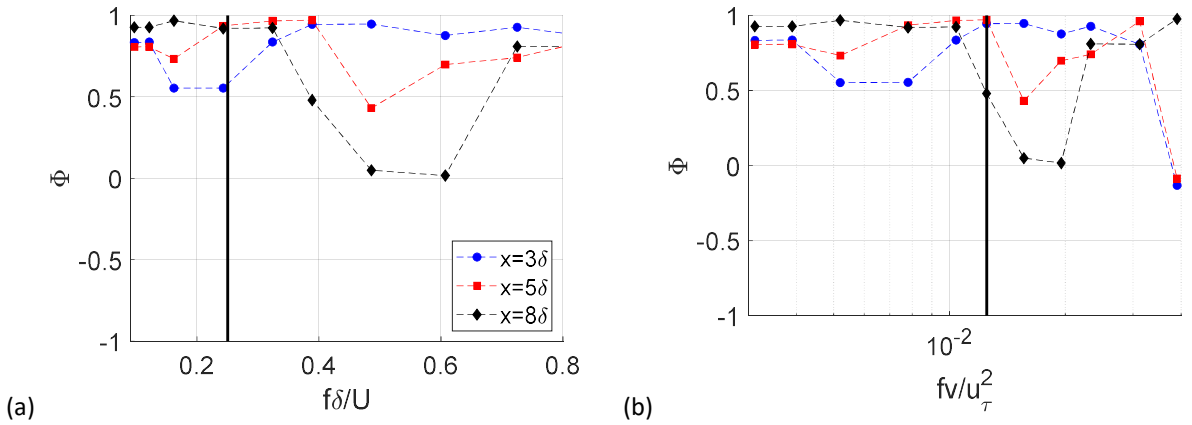

Figure 3. (a) Outer scaled frequency response for different streamwise locations. The vertical line marks $f_{LS}^* = 0.25$. (b) Inner scaled frequency response. The vertical line marks $f_{SS}^+ = 0.011$. $H^+ = 200$.

V. Results

With the key parameters of the actuator optimized, further analysis of the effect of the actuator on the turbulent boundary layer was performed. First, the canonical boundary layer, that is, without the actuator plate, was measured with the hot-wire at each measurement location to establish a baseline before adding the passive effect of the physical actuator plate or the active effect of applying plasma forcing.

The canonical mean velocity profile and turbulence intensity profiles at the streamwise measurement location of $x = 5\delta$ can be seen in Figure 4(a). There is a well-defined log-linear region in the mean velocity profile from $y^+ = 50 - 200$ and near the wall the velocity profile approaches the linear scaling of the viscous sublayer, though the measurements do not extend into the sublayer in this case. The peak in the turbulence intensity is around $y^+ = 16$ and has an error in normalized amplitude of approximately 20% due to the spatial averaging effect of the finite hot-wire length as mentioned in the experimental setup [18].

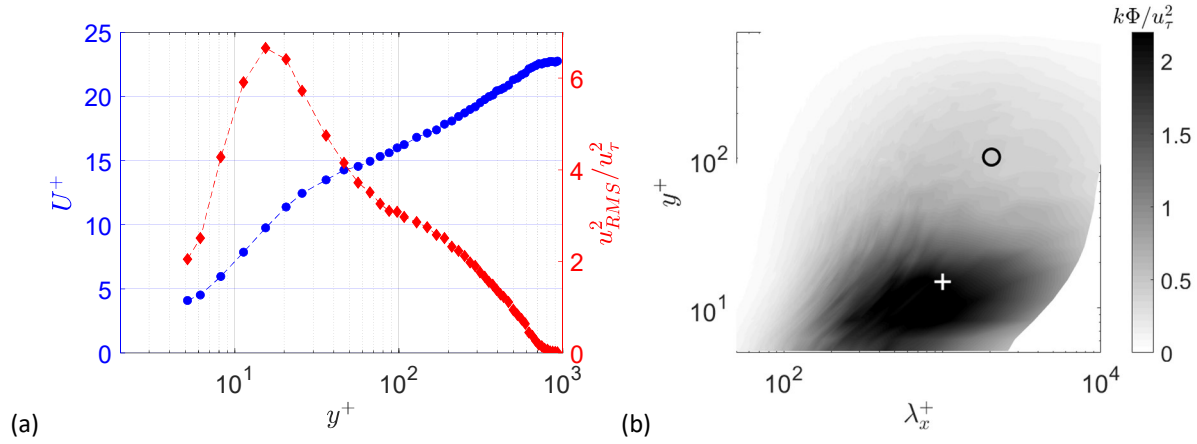

Figure 4. (a) Mean velocity and turbulence intensity profiles for canonical boundary layer. (b) Premultiplied streamwise energy spectra for canonical boundary layer at $x = 5\delta$. Cross marks inner peak ($y^+ = 15, \lambda_x^+ = 1000$). Open circle marks expected location of outer peak ($y^+ = 3.9Re_\tau^{1/2}, \lambda_x^+ \approx 2000$) for $Re_\tau = 690$.

The premultiplied streamwise wavenumber-frequency energy spectra for a single measurement location of $x = 5\delta$ is presented in Figure 4(b). The near-wall or inner energy peak aligns well with the expected location of $y^+ = 15, \lambda_x^+ = 1000$ marked by the white cross [1]. The expected spectral location of the natural LSS at the geometric center of the log-region for sufficiently large Reynolds numbers [3] is indicated by a circle in Figure 4(a). At the relatively low Reynolds number of $Re_\tau = 690$ in this experiment, there is no natural coherent large-scale structure present. There are less organized and less energetic large-scale motions present in the boundary layer which result in the diffuse lobe extending away from the wall and towards longer streamwise wavelengths. The streamwise wavelength of the naturally-occurring LSS has been reported in the range of $3 - 6\delta$ in other studies [1] [3] and the streamwise wavelength of $\lambda_x = 3\delta$ ($\lambda_x^+ = 2000$) specifically is identified by the open circle in Figure 4(b). In addition to the quantitative agreement of the premultiplied spectra to expected values, there is also qualitative agreement with other experiments at similar sufficiently low Reynolds numbers [3].

After the canonical baseline was established, the actuator plate was added to the setup without any active plasma forcing. Since the presence of the plate alone will modify the boundary layer, as discussed in the introduction, the changes in the baseline flow were quantified before evaluating the effect of the plasma forcing. The modified mean velocity profile, turbulence intensity and the skewness for two streamwise locations can be seen in Figure 5 as open symbols. For comparison, the same quantities for the canonical boundary layer are also shown in Figure 5 as a solid line. At the actuator plate's wall-normal location, marked by the dotted line, there is a local decrease in mean velocity,

shown in inner unit scaling in Figure 5(a) and in outer unit scaling in Figure 5(b), and a local increase in turbulence intensity, shown in Figure 5(c). These effects are representative of the plate's wake. The skewness profiles at the actuator location, shown in Figure 5(d), approaches zero downstream of the plate; this is an expected behavior at the center of the plate's wake. Moving downstream, the mean velocity deficit and increased turbulence intensity around the actuator plate location tend to recover towards the canonical profile. Below the actuator plate there is a consistent decrease in turbulence intensity at $x = 5\delta$ compared to $x = 1.5\delta$. The profile of skewness appears to be constant between the two measurement locations.

The wake created by the presence of the actuator plate was extracted from the modified boundary layer profile, $U_{plate}(y)$ by subtracting the canonical boundary layer profile, $U_{canon}(y)$, from it. Wake profiles for the first three measurement locations, normalized by the wake half-width, *w*, and velocity deficit, ΔU_{max}, are presented in Figure 6(a). The streamwise development of the wake half-width and maximum velocity deficit are also presented in Figure 6(b), along with the expected streamwise evolution for two-dimensional wakes, indicated by solid and dashed lines, respectively. The wake half-width is expected to grow as $w \sim x^{0.5}$ while the maximum velocity deficit is expected to decay as $\Delta U_{max} \sim x^{-0.5}$. Collectively, these figures demonstrate that immediately downstream of the actuator, and persisting farther downstream, the wake from the actuator plate follows a canonical plane wake development [24].

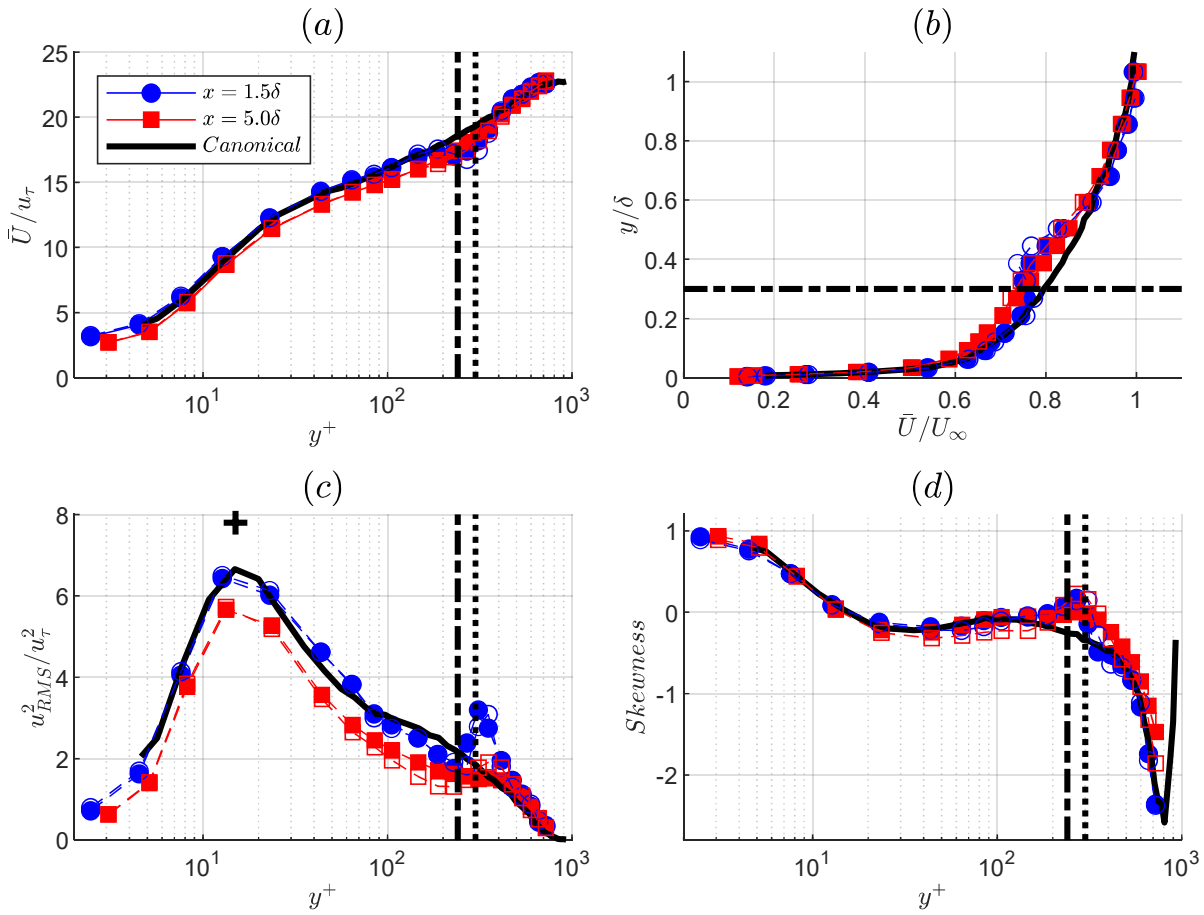

Figure 5. Profiles of (a) inner scaled mean velocity (b) outer scaled mean velocity (c) turbulence intensity and (d) skewness at $x = 1.5\delta$ (blue) and $x = 5\delta$ (red). Canonical (solid line), plate only (open symbols) and plasma on (filled symbols). The vertical dot-dash line marks the actuator height $H = 0.3\delta$ ($H^+ = 200$). Vertical dotted line marks effective plasma forcing location ($H_P^+ = 265$).

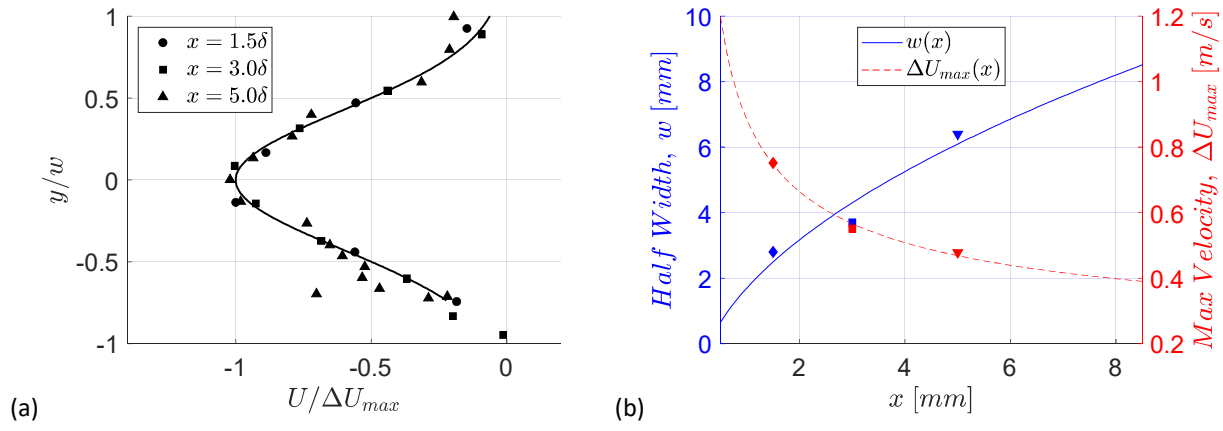

Figure 6. (a) Profiles of wake velocity deficit behind plate ($U_{plate}(y) - U_{canon}(y)$) normalized by half width and maximum velocity deficit. (b) streamwise evolution of wake half width and velocity deficit. $H^+ = 200$.

The premultiplied spectra for the plate only case (no active plasma) is presented in Figure 7. The spectra appear very similar to the premultiplied spectra for the canonical boundary layer, presented in Figure 4(b). Comparing the energy spectra seems to indicate that the presence of the plate does not significantly change the organization of structures within the boundary layer.

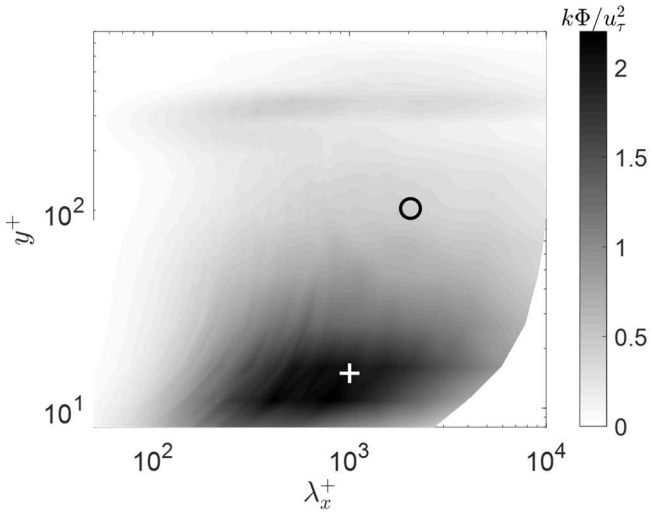

Figure 7. Premultiplied energy spectra for plate-only case (plasma off) on at $= 1.5\delta$. $H^+ = 200$. Cross marks inner peak ($y^+ = 15, \lambda_x^+ = 1000$). Open circle marks expected outer peak ($y^+ = 3.9Re_\tau^{1/2}, \lambda_x^+ \approx 2000$).

The full effect of the actuator plate on the baseline flow at different streamwise locations can be more easily seen by looking at the difference in premultiplied spectra between the canonical and plate only (plasma off) cases, presented in Figure 8. The locations of the inner peak and the expected outer peaks are also indicated in Figure 8. By examining the discrepancy between the plate only and canonical cases in Figure 8(a) at the streamwise location of $x = 1.5\delta$, there is a decrease in the energy of large wavelength motions and an increase in the energy of smaller wavelength motions, $\lambda_x^+ < 500$. This behavior is consistent with the plate inhibiting the formation of large-scale structures and the generation of smaller scale structures in the plate's wake as described in other studies of flat plate manipulators [11] [12]. This flat plate effect persists downstream but starts to weaken and spread in the wall-normal direction farther downstream of the actuator at $x = 5\delta$, as shown in Figure 8(b). This is consistent with the spreading of the wake generated by the plate. There is also an immediate suppression of energy around the inner peak location at the closest streamwise location $x = 1.5\delta$, see Figure 8(a), which recovers farther downstream, as the boundary layer has time to respond to the presence of the plate.

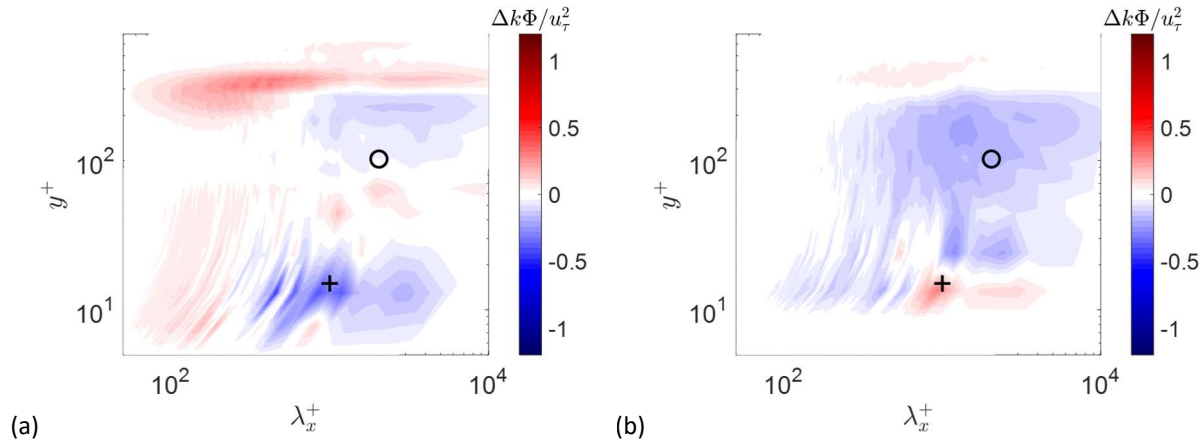

Figure 8. Discrepancy between plasma off and canonical premultiplied spectra at (a) $x = 1.5\delta$ and (b) $x = 5\delta$. $H^+ = 200$. Cross marks inner peak ($y^+ = 15, \lambda_x^+ = 1000$). Open circle marks expected outer peak ($y^+ = 3.9Re_\tau^{1/2}, \lambda_x^+ \approx 2000$).

To quantify the effect of the plasma forcing, the velocity profiles downstream of the plasma-induced jet were first measured in still air using a hot-wire to determine the jet statistics. The results, normalized by the local jet half-width and the local maximum jet velocity, are shown in Figure 9. The jet velocity profile, shown in Figure 9(a), was found to have a Gaussian shape and followed a canonical growth pattern in still air, as demonstrated in in Figure 9(b). The expected jet half-width growth is $w \sim x$ while the jet maximum velocity is expected to decay as $u_{max} \sim x^{-0.5}$. The maximum jet velocity was approximately 5 m/sec immediately downstream of the actuator. However, it was also noted that there was a significant change in the observed jet velocity profile when it was introduced within the turbulent boundary layer, as shown in Figure 10. The maximum jet mean velocity, which was extracted by subtracting the plate only mean velocity from the plasma on mean velocity, was 0.3 m/sec or $\sim 0.04U_\infty$, which is much less than maximum jet velocity in still air. Thus, the accelerating effect of the plasma jet is not as pronounced when the air is moving in the boundary layer and the plate's wake is affecting the flow immediately downstream. In spite of this, for the presented experiments it was determined that the plasma jet was sufficiently strong. It is also important to note that the plasma jet's effective origin was found to be approximately 3 mm above the plate's surface which makes the effective height of the synthetic motions produced by the actuator closer to $H^+ = 265$. This actual location of the plasma jet is marked by the dotted line in Figure 5. This notion is also important for correctly modeling the actuated flow.

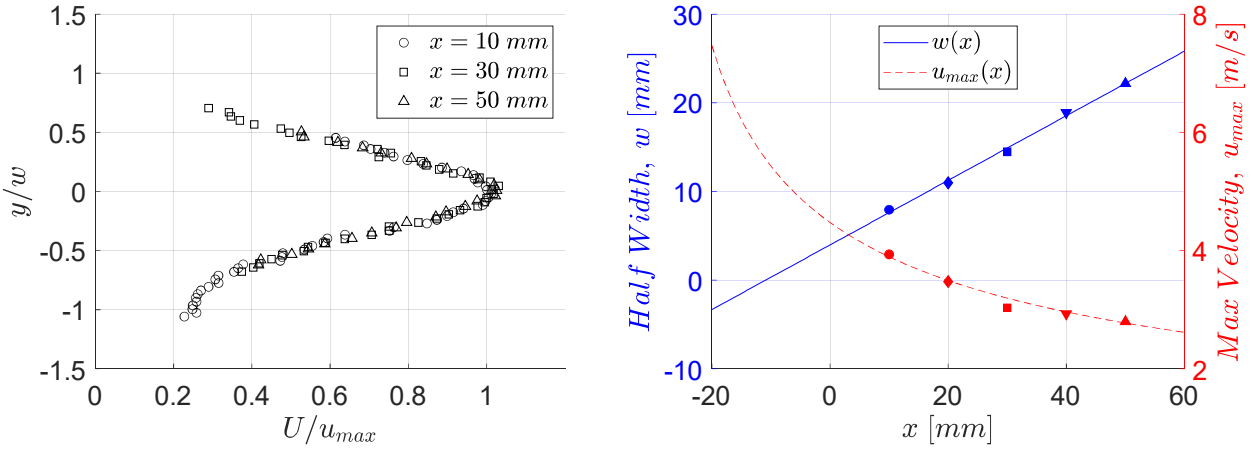

Figure 9. (a) Profiles of jet mean velocity in quiescent air normalized by half width and maximum velocity. (b) streamwise evolution of jet half width and maximum velocity. $H^+ = 200,\ f_P = 80\ Hz$.

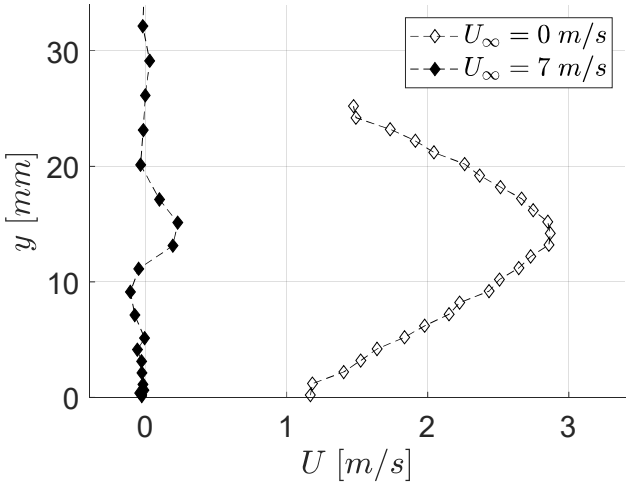

Figure 10. Profiles of jet mean velocity in quiescent air $U_\infty = 0m/s$ and inside TBL ($U_{plasma}(y) - U_{canon}(y)$) with $U_\infty = 7m/s$. $H^+ = 200,\ f_P = 80\ Hz$.

Once the modified baseline (plate only) was established, the effect of the plasma forcing on the boundary layer was studied. First, the mean velocity, turbulence intensity and skewness for the plasma on case are presented in Figure 5 as filled symbols. At the actuator height, there are small changes to the amplitude of the velocity deficit, the peak in turbulence intensity and the amplitude of the skewness. These peaks have also been shifted slightly towards the wall due to the presence of the plasma jet on the top side of the actuator plate. These results are expected, as the lack of significant change in statistical quantities has been observed with other actuators where the induced perturbations

affect boundary layer dynamics with little relative change in statistical quantities [15]. The premultiplied spectra of the actuated TBL is shown in Figure 11. The energy signature of the synthetic LSS produced by ALSSA can be seen in the region of $y^+ = 265, \lambda_x^+ = 1600$ ($\lambda_x = 2.5\delta$). There is also a narrow band of higher than canonical energy that extends from this outer peak towards the wall.

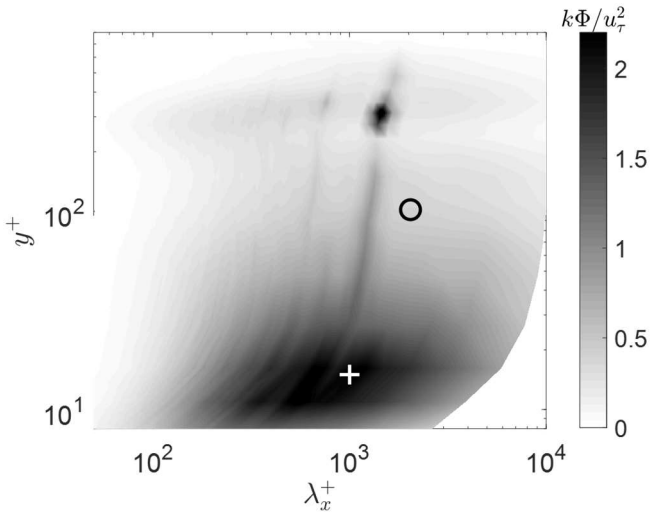

Figure 11. Premultiplied energy spectra for plasma on at $= 1.5\delta$. $H^+ = 200$. Cross marks inner peak ($y^+ = 15, \lambda_x^+ = 1000$). Open circle marks expected outer peak ($y^+ = 3.9Re_\tau^{1/2}, \lambda_x^+ \approx 2000$).

The discrepancy in premultiplied spectra between the plasma on and plasma off (plate only) cases at different streamwise locations can be seen in Figure 12. There is a clear contribution to the energy spectra at the wavelengths associated with the plasma forcing frequency across the boundary layer. The strongest contribution is at the actuator height close to the actuator, as shown in Figure 12(a), and there is an additional elongated spectral ridge that extends though the near wall region. This signature of the large-scale motions from the actuator is similar to the signature of the boundary layer response to dynamic roughness perturbations presented in [15], which originate within the log-region closer to the wall. At the downstream location of $x = 5\delta$, shown in Figure 12(b), the peak in energy has shifted and is concentrated mostly in the log-region. There are also changes in the near-wall energy peak at both downstream locations, which is an indication that the large-scale motions are interacting with the near-wall small-scale structures. Similar to the results in [16], the discrepancies in premultiplied spectra observed here show the receptivity of the TBL to large-scale perturbations. In this case, energy introduced through the synthetic large-scale motions in the outer layer is also changing the energy composition near the wall through some outer-inner interaction mechanism.

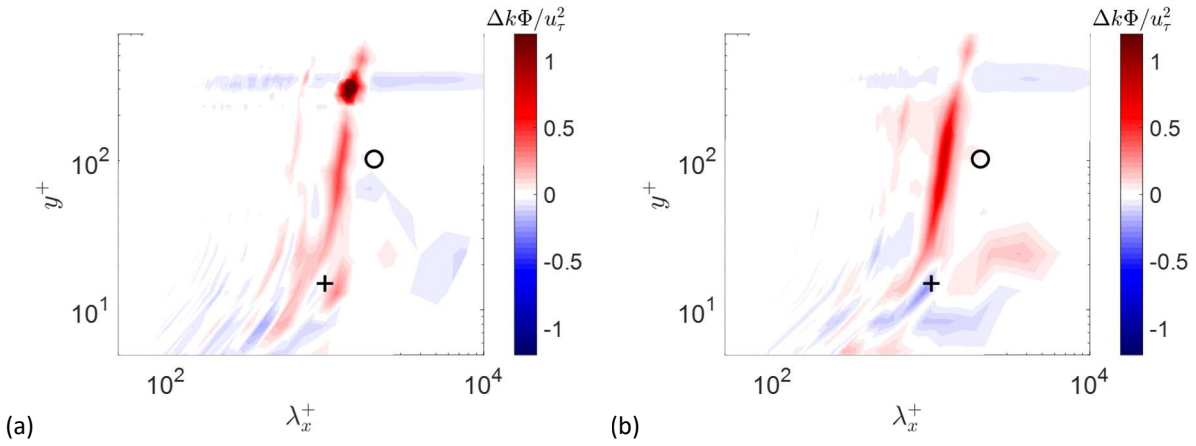

Figure 12. Discrepancy between plasma on, $f_P = 80\ Hz$, and plasma off premultiplied spectra at (a) $x = 1.5\delta$ and (b) $x = 5\delta$. (c) full plasma on spectra. $H^+ = 200$. Cross marks inner peak ($y^+ = 15, \lambda_x^+ = 1000$). Open circle marks predicted outer peak ($y^+ = 3.9Re_\tau^{1/2}, \lambda_x^+ \approx 3\delta$).

With the statistical comparison between the baseline flows established, the phase-locking method, shown earlier, was implemented to analyze the effects most directly related to the disturbances introduced by the periodic plasma forcing. To begin with, maps of the modal velocity and residual turbulence were computed for each streamwise measurement location. Phase maps of the modal velocity at streamwise locations of $x = 1.5\delta$ and 3δ are presented in Figure 13(a,b) and the results at streamwise locations of $x = 5\delta$ and 8δ are presented in Figure 14(a,b). There is a strong modal component of velocity at the actuator location, but there is also a significant modal velocity contribution that extends all the way towards the wall. The phase and the orientation of the regions of positive modal velocity change moving downstream are consistent with the change in convective velocity across the boundary layer. The shapes of these regions match well with both the amplitude and predicted shapes from spatial input-output analysis [25] and other experiments, where large-scale perturbations were introduced near the wall [16]. It is of note that in this experiment the modal velocity pattern is well established immediately downstream of the plate, allowing for analysis of this region close to the actuator and extending downstream where the boundary layer adjusts to the synthetic LSS. The fluctuations in modal velocity around the actuator location decay slightly downstream while the fluctuations induced in the log-region appear to remain constant despite downstream location.

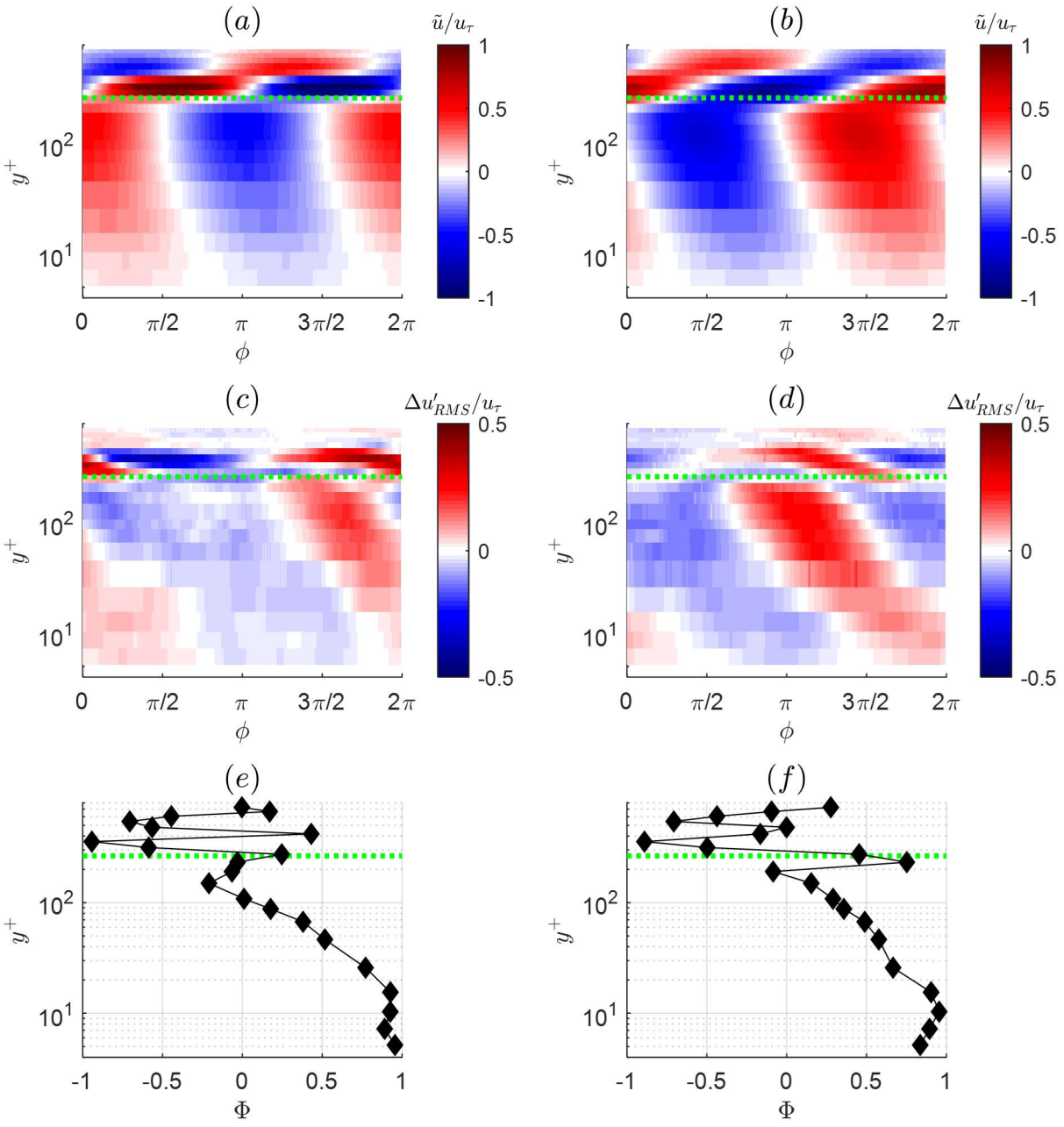

Figure 13. (a,b) Phase maps of modal velocity (c,d) phase maps of residual turbulence (e,f) modulation function Φ. (a,c,e) $x = 1.5\delta$ (b,d,f) $x = 3\delta$. $H^+ = 200, f_P = 80\ Hz$. The horizontal dashed line represents the plasma forcing location.

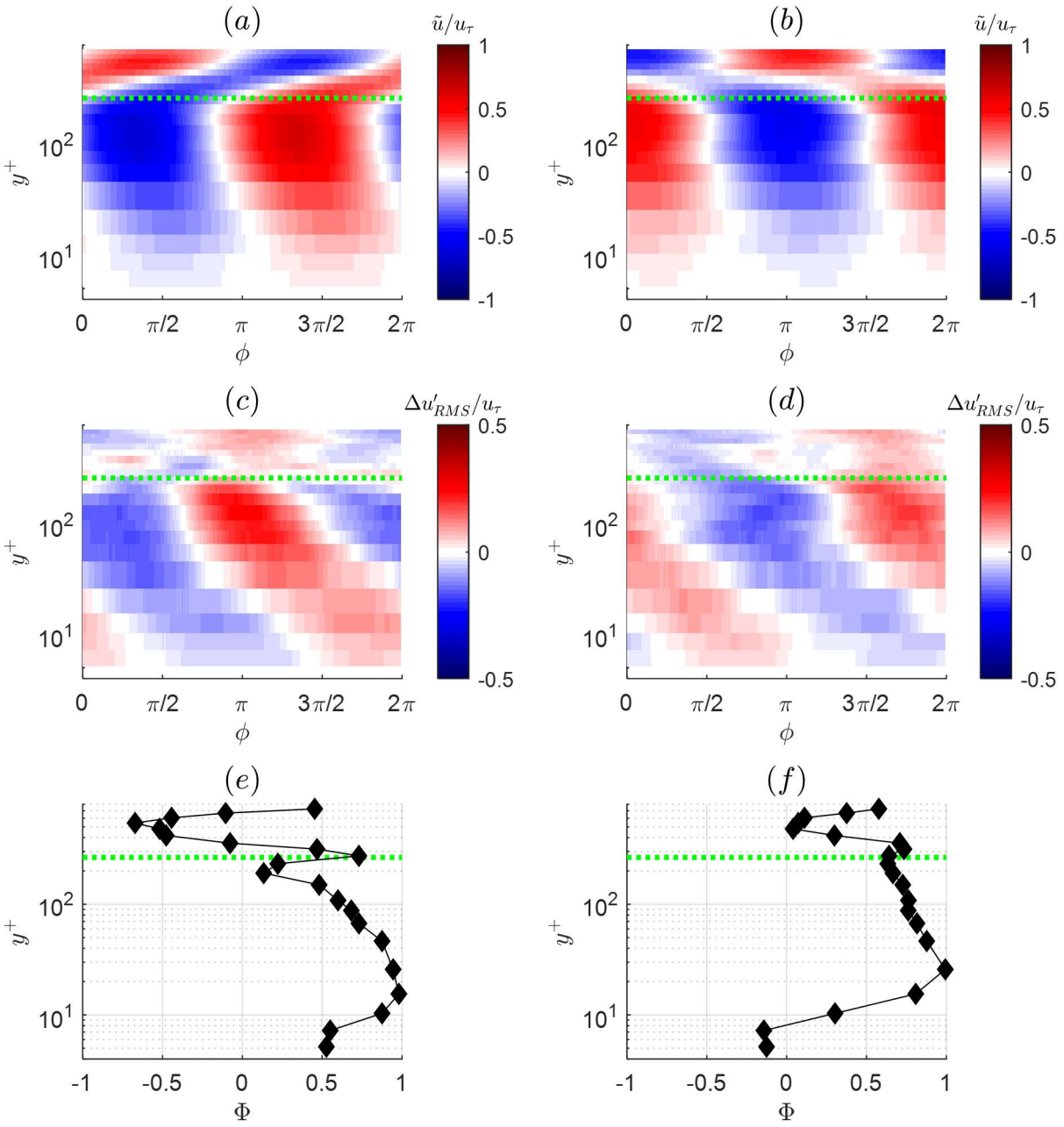

Figure 14. (a,b) Phase maps of modal velocity (c,d) phase maps of residual turbulence (e,f) modulation function Φ. (a,c,e) $x = 5\delta$ (b,d,f) $x = 8\delta$. $H^+ = 200, f_P = 80\ Hz$. The horizontal dashed line represents the actuator location.

The phase maps of residual turbulence at different streamwise locations are shown in Figure 13(c,d) and Figure 14(c,d). They follow a trend, similar to the modal velocity results, where there are strong fluctuations near the actuator location, but now directly below those fluctuations aligned in phase there is another region of strong fluctuations in

the residual turbulence. The positive fluctuations in residual turbulence above the plate are a signature of the convecting synthetic large-scale motions and the regions within the log or near-wall region are modulated or reorganized small-scale turbulence. This reorganized region or region of modulated turbulence also evolves downstream, locking into a preferred orientation as it approaches the farthest downstream measurement location, even as the signature of the synthetic motions above begin to diminish. The inclination of this region of modulated turbulence with respect to the wall also matches well with the observed inclination of LSS in higher Reynolds number boundary layers [3]. These phase maps of residual turbulence and modal velocity demonstrate the modulating effect of the synthetic large-scale motions and the persistence of the synthetic large-scale structure's influence on the boundary layer even at the farthest downstream measurement locations.

Profiles of the modulation coefficient Φ are shown in Figure 13(e,f) and Figure 14(e,f). At the measurement locations closest to the actuator, there is a positive peak in the modulation coefficient in line with the location of plasma forcing. There is also a peak in the modulation coefficient in the near-wall region of the boundary layer. This near-wall peak shows that fluctuations in the modal velocity and residual turbulence are in phase and highlights the modulation effect that the synthetic LSS has even in the near wall region. Farther downstream the peak in modulation persists at the location of plasma forcing. The peak that was confined mostly to the near-wall region at earlier downstream locations has now shifted and more broadly spans the log-region at farther downstream locations. This is consistent with the observation of the modal velocity and residual turbulence independently as well as the reorganization of energetic structures as seen in the premultiplied spectra.

The phase maps of modal velocity from sequential downstream locations can also be used to determine the phase speed of large-scale disturbances which are phase-locked with the plasma forcing. The phase speed is estimated by determining the time delay, t_n (related to phase by Equation 2), of certain features in the modal velocity signal, like a local minimum or a maximum, as they arrive at different downstream measurement locations. Using the relationship between phase and time from Equation 2 and appropriately adjusting the time with additional actuation period delays at the farther downstream locations, the total time delay from the beginning of the actuation cycle can be found. The average phase speed between measurement locations can then be estimated using the difference in time delay and the difference in streamwise location between any two measurement locations. It is expected that the modal velocity component just above the actuator will be continuous due to the periodic and strong fluctuations induced by the synthetic LSS when comparing between streamwise locations. If the phase speed is correctly computed the modal

velocity at a specific wall-normal location can be converted from phase to pseudo-space using Equation 5 and the signal will be continuous as demonstrated in Figure 15(b).

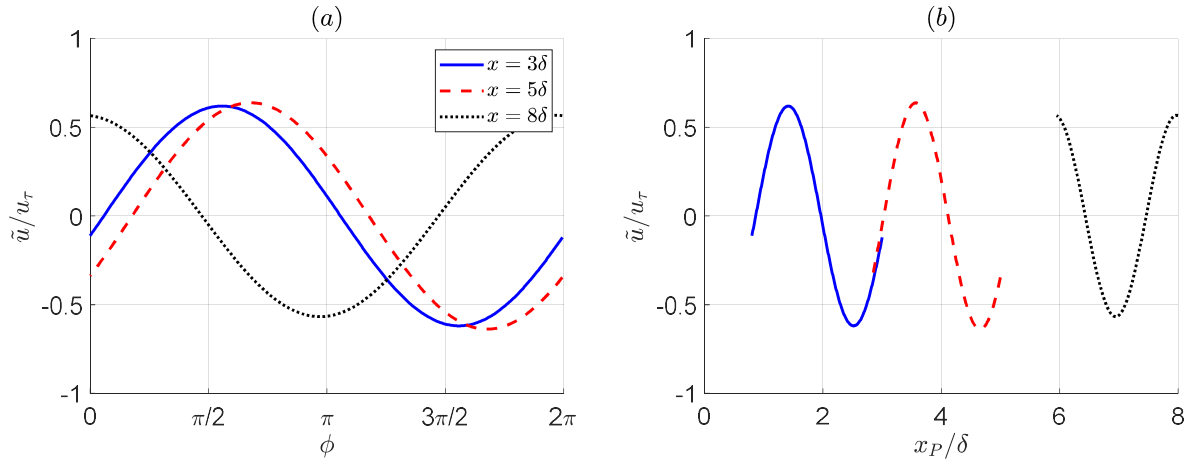

Figure 15. Streamwise modal velocity in (a) phase space and (b) reconstructed pseudo-space. $H^+ = 200, f_P = 80\ Hz$.

In Figure 15(a) the phase dependent modal velocities from each measurement location are shown and in Figure 15(b) the reconstructed modal velocity can be seen where the signal now appears continuous. This procedure can be applied across the entire boundary layer to find the phase speed of the phase-locked fluctuations. The results of this phase speed analysis are shown in Figure 16. As shown in Figure 16, the phase speed below the actuator location is approximately constant across all wall-normal locations. At the closest location to the plate, see Figure 16(a), the phase-speed below the actuator is approximately equal to the local mean velocity at the actuator location, $u_\varphi = 17u_\tau = 0.75U_\infty$, indicating that fluctuations in phase-locked quantities are a direct effect of modulation by the synthetic LSS. Above the actuator height, the phase speed begins to follow the profile of the mean velocity locally. In Figure 16(b,c) the phase-speed below the actuator is increasing but is still equal to the local mean velocity at the height of actuation. By the farthest downstream location shown in Figure 16(d) the streamwise growth in phase speed below the actuator appears to be reaching an asymptote. The phase speed at and above the actuator also begins to be consistently higher than the local mean velocity. This observation suggests that the phase-speed of fluctuations below the actuator are strongly correlated with the speed of the synthetic large-scale structures produced by the actuator.

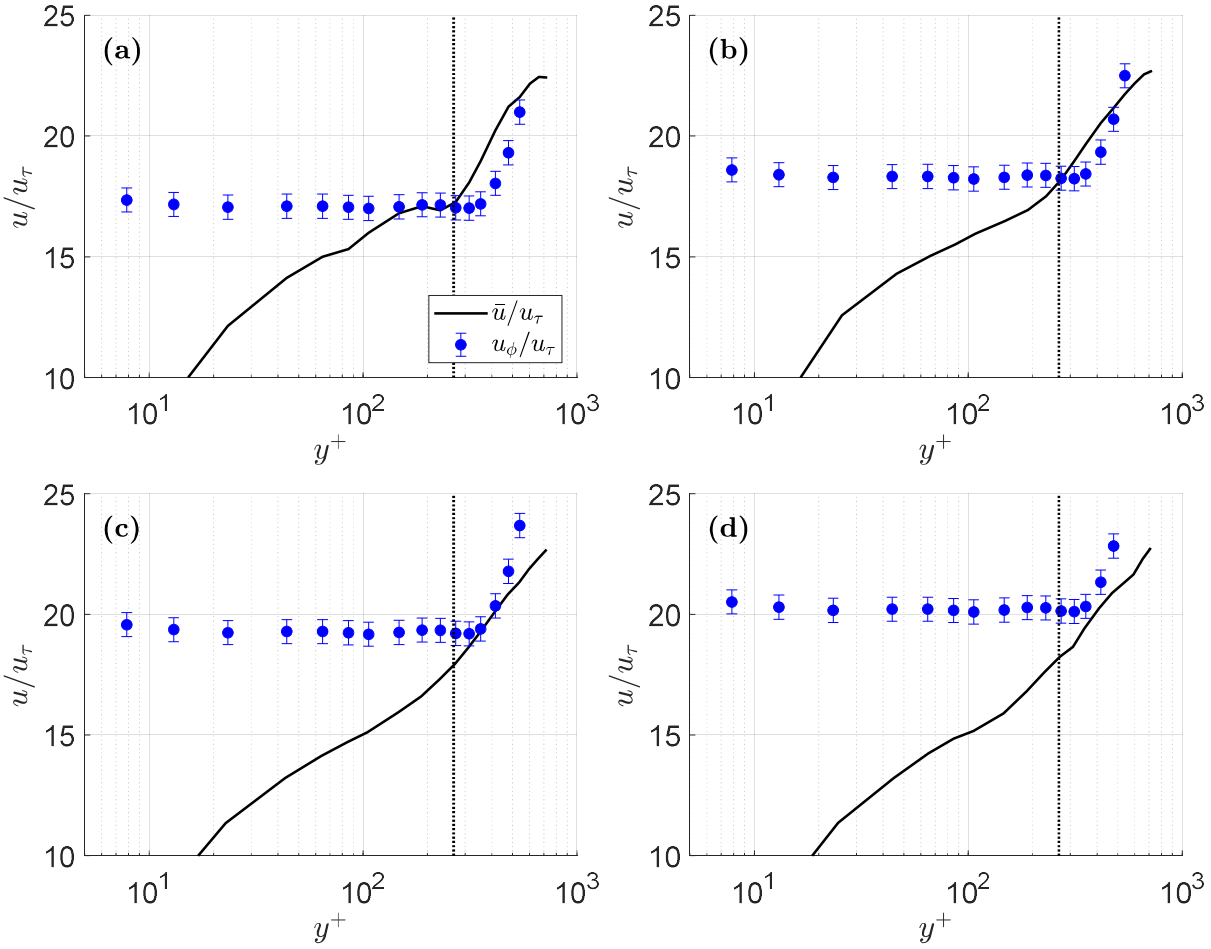

Figure 16. Phase speed of large-scale disturbances phase-locked with plasma forcing at (a) $x = 1.5\delta$, (b) $x = 3\delta$, (c) $x = 5\delta$, (d) $x = 8\delta$. $H^+ = 200, h = 0.3\delta, f_P = 80\ Hz$. Dashed line represents actuator location.

Using the estimated phase speed as an effective local convective velocity, U_c , and applying Taylor's frozen field hypothesis,

$$x_p = x_{meas} - \frac{\varphi}{2\pi}\frac{1}{f_p}U_c \tag{5}$$

the phase of each of the previous measurements was converted into a pseudo spatial streamwise coordinate, x_P. A pseudo spatial reconstruction of the streamwise modal velocity, the wall-normal modal velocity, and the residual turbulence for the whole flow field downstream of the actuator is presented in Figure 17. In Figure 17(a,b) the reconstructions of streamwise modal velocity and residual turbulence show two distinct wall-normal regions of phase-locked fluctuation. In the streamwise modal velocity, fluctuations below the actuator appear to lead changes above

the actuator location. On the other hand, positive changes in the residual turbulence below the actuator appear to be aligned with positive changes above the actuator, but the regions are spatially distinct. The wall-normal modal velocity, $\tilde{v}$, was computed by integrating the two-dimensional continuity equation in the wall-normal direction and imposing a no slip condition at the wall,

$$\tilde{v}(y, x_p) = -\int_0^y \frac{\partial \tilde{u}(y, x_p)}{\partial x_p} dy. \tag{6}$$

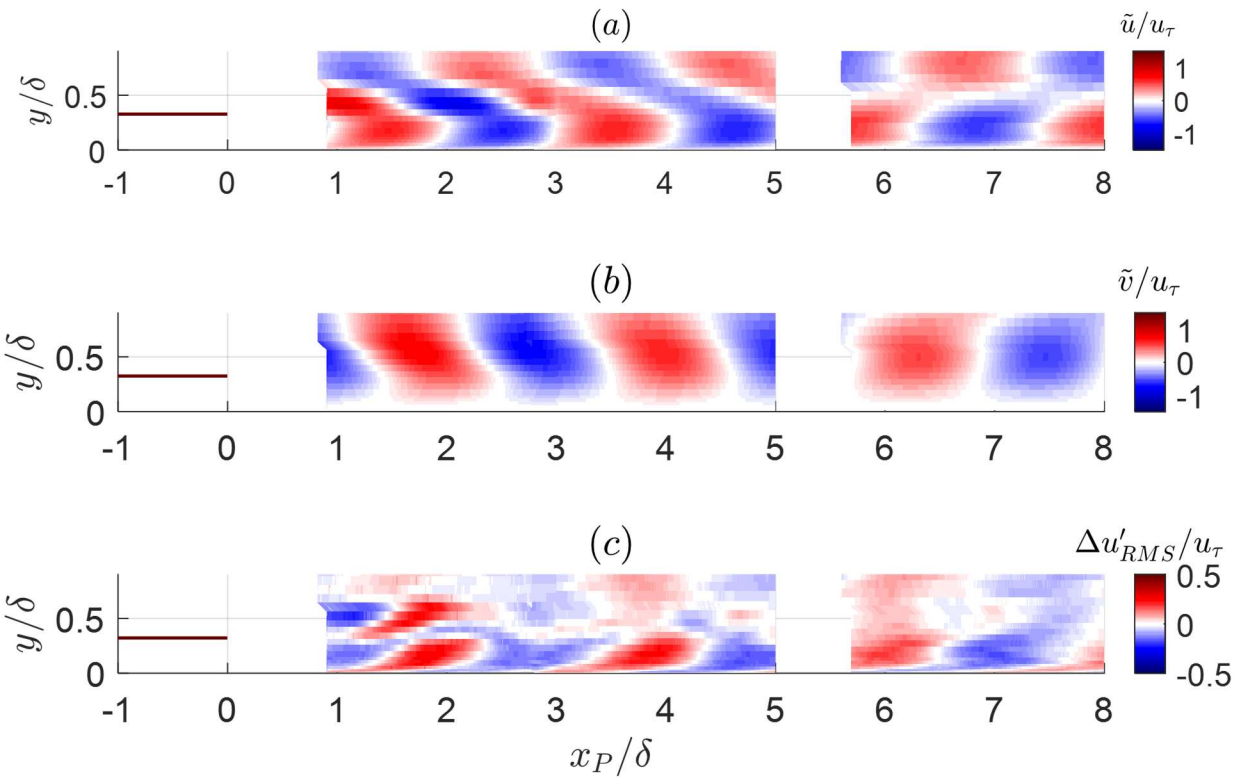

Figure 17. Pseudo-spatial reconstructions of (a) streamwise modal velocity (b) wall-normal modal velocity and (c) residual turbulence. $H^+ = 200, f_p = 80\ Hz$.

Because the convective velocity of the streamwise modal velocity is essentially constant over the entire boundary layer we expect that using the continuity condition to compute the wall-normal component will give a reasonable approximation. This was confirmed by the results of the spatial input output analysis where similar shapes, phase and amplitude were observed for the changes in modal wall-normal velocity [25]. The wall-normal modal velocity does

not have the same distinct wall-normal regions but instead appears in evenly spaced and periodic columns of fluctuations. This pseudo-spatial reconstruction gives an alternative picture of the flow field downstream of the actuator and the regions of modulated turbulence can be compared in space instead of phase.

The phase maps of modal velocity and residual turbulence can also be used to quantify the modulating effect of the large-scale structures through a modulation coefficient, Φ which was defined in Equation 4. Figure 18 shows the profile of the modulation coefficient at all streamwise locations. At the actuator location, there is a large positive correlation directly below the plate and a negative correlation above the plate due to the meandering wake behind the plate. The turbulence intensity deficit below the plate and the turbulence intensity increase produced on top of the plate fluctuate with the plasma forcing, in a wall normal meandering motion, creating the distinct profile of Φ in that region. There is also a region of strong positive modulation near the wall. This region is an indication that the near-wall turbulent structures are in fact being modulated or reorganized by synthetic large-scale motions. The trend moving downstream is that the region of positive modulation is growing and becoming more positive. A similar trend has been documented, as the Reynolds number of a canonical boundary layer is increased [2]. A quasi-steady theory, proposed in [26], hypothesizes that the flow should react to small large-scale velocity changes in a linear manner. Using the appropriately scaled modal velocity and residual turbulence components near the wall at each streamwise location, it was found that they are in fact linearly related in general and the relationship becomes more linear and homogeneous moving downstream. The increase of correlation between scales, the changing orientation of the region of modulated turbulence, and the increasingly linear response moving downstream collectively suggest that by introducing a synthetic large-scale structure into a low Reynolds number the boundary layer, it gradually responds and behaves dynamically in a manner similar to a higher Reynolds number boundary layer.

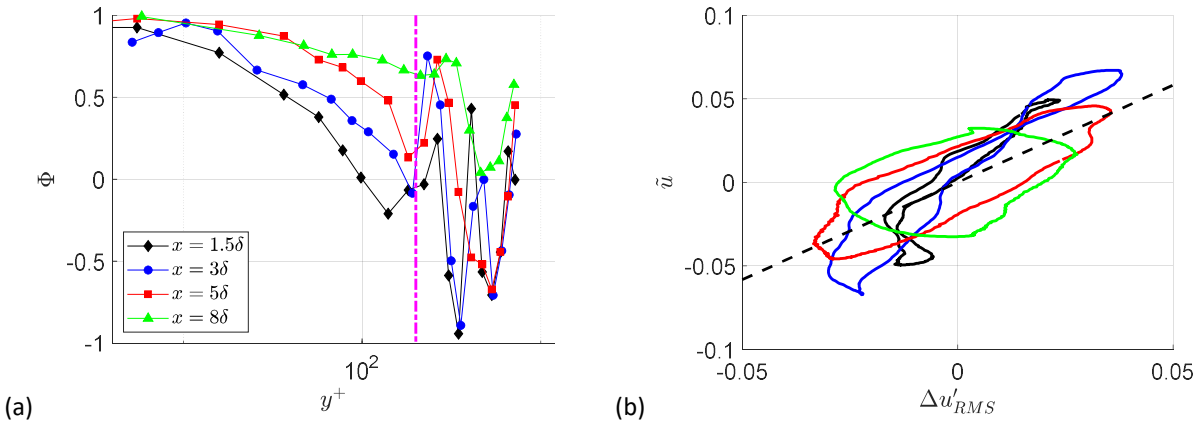

Figure 18. (a) Streamwise evolution of the modulation coefficient Φ (b) streamwise evolution of the correlation between modal velocity and residual turbulence at $y^+ = 20$. $H^+ = 200, f_P = 80\ Hz$.

VI. Conclusions

Experimental studies of a zero-pressure gradient turbulent boundary layer response to synthetic, periodic large-scale structures were conducted using hot-wire anemometry. A plasma-based active flow control device was placed within the boundary layer in order to introduce periodic large-scale motions into the outer region. The boundary layer Reynolds number was low enough ($Re_\tau = 700$) that no naturally occurring coherent large-scale structures were present in this region. This approach essentially uncoupled the non-linear interaction between the large-scale structure and the near-wall turbulence present in higher Reynolds number boundary layers and allowed the systematic study of the effect of the large-scale structure on the near-wall turbulence. The width of the actuator was sufficient to ensure that the introduced synthetic motions are two dimensional and the large-scale flow structure downstream of the actuator is essentially spanwise uniform. The forcing frequency of the synthetic large-scale structure was chosen to produce the maximum modulating effect on the smaller near-wall scales. In this sense the forcing frequency matched the most receptive frequencies of motion in the near wall region, which corresponded to characteristic scales of the near-wall cycle. The actuator was also positioned such that the synthetic large-scale structure was introduced just outside of the log-region. This wall-normal location was shown to cause the largest interaction between the large-scale motions and small scales near the wall. The phase locked analysis was used to quantitatively measure the modulating effect of the synthetic large-scale motions on the near-wall turbulence. It was demonstrated that the structures produced by the actuator modulated turbulent structures near the wall and in the log-region of the boundary layer. This modulating effect persisted for several boundary layer thicknesses downstream of the actuator even as the

organized large-scale motions in the outer region diminished. These regions of modulated turbulence occurred directly below peaks in residual turbulence generated by the plasma actuator as they convect downstream. The near-wall modulated regions have very similar angular orientation to the naturally occurring structures found in higher Reynolds number boundary layers. Wall-normal profiles of the phase speed were also extracted from the data. The phase speed was found to be constant below the actuator and was equal to the convective speed of the synthetic structure, suggesting a strong coupling between the fluctuations below the actuator and the speed of the synthetic large-scale structures produced by the actuator. Overall, the observed changes demonstrate the receptivity of the boundary layer to large-scale forcing as the boundary layer quickly adjusted to the presence of the synthetic large-scale structure.

The results of this experimental investigation showed that the synthetic, periodic large-scale structure introduced by the plasma actuator had a very similar dynamic effect on the turbulent boundary layer as the naturally occurring large-scale structures in the higher Reynold number boundary layers. Thus, the presented approach would be useful to further study the non-linear interaction between the large-scale structure and the near-wall turbulence in turbulent boundary layers, as well as to explore various flow control approaches to manipulate boundary layers.

Funding Sources

This work is supported by the Office of Naval Research, Grant number N00014-18-1-2534. The U.S. Government is authorized to reproduce and distribute reprints for governmental purposes notwithstanding any copyright notation thereon.

References

[1] M. Guala, S. E. Hommema and R. J. Adrian, "Large-scale and very large-scale motions in turbulent pipe flow," *J. Fluid Mech.,* vol. 554, pp. 521-542, 2006.

[2] R. Mathis, N. Hutchins and I. Marusic, "Large-Scale Amplitude Modulation of the Small-Scale Sturcutres in Turbulent Boundary Layers," *J. Fluid Mech.,* vol. 658, pp. 311-336, 2009.

[3] N. Hutchins and I. Marusic, "Large-scale influences in near-wall turbulence," *Phil. Trans. R. Soc. A,* vol. 365, pp. 647-664, 2007.

[4] S. K. Robinson, "Coherent Motions in the Turbulent Boundary Layer," *Ann. Rev. Fluid Mech.,* vol. 23, pp. 601-639, 1991.

[5] R. J. Adrian, C. D. Meinhart and C. D. Tomkins, "Vortex organization in the outer region of the turbulent boundary layer," *J. Fluid Mech.,* vol. 422, pp. 1-53, 2000.

[6] C. M. de Silva, N. Hutchins and I. Marusic, "Uniform momentum zones in turbulent boundary layers," *J. Fluid Mech.,* vol. 786, pp. 309-331, 2016.

[7] I. Marusic and J. P. Monty, "Attached Eddy Model of Wall Turbulence," *Ann. Rev. Fluid Mech.,* vol. 51, pp. 49-74, 2019.

[8] D. M. Schatzman and F. O. Thomas, "An experimental investigation of an unstready adverse pressure gradient turbulent boundary layer: embedded shear layer scaling," *J. Fluid Mech.,* vol. 815, pp. 592-642, 2017.

[9] D. E. Coles and E. A. Hirst, "Comutation of Turbulent Boundary Layers: Compiled Data," in *AFOSR-IFP*, Stanford University, 1968.

[10] P. Ranade, S. Duvuuri, B. McKeon, S. Gordeyev, K. Christensen and E. J. Jumper, "Turbulence Amplitude Amplification in an Externally Forced, Subsonic Turbulent Boundary Layer," *AIAA Journal,* vol. 57, pp. 3838-3850, 2019.

[11] T. C. Corke, Y. Guezennec and H. M. Nagib, "Modification in drag of turbulent boundary layers resulting from manipulation of large-scale strucutres," NASA CR-3444, 1981.

[12] A. E. Smith and S. Gordeyev, "Aero-Optical Mitigation of Turbulent Boundary Layers Usin Large-Eddy Break-Up Devices," in *AIAA SciTech*, 2014.

[13] A. M. Savill and J. C. Mumford, "Manipulations of turbulent boundary layers by outer-layer devices: skin-friction and flow-visualization results," *J. Fluid Mech.,* vol. 191, pp. 389-418, 1988.

[14] S. Duvuuri and B. McKeon, "Phase relations in a forced turbulent boundary layer: implications for modelling in high Reynolds number wall turbulence," *Phil. Trans. A,* vol. 375, 2017.

[15] I. Jacobi and B. McKeon, "Dynamic roughness perturbation of a turbulent boundary layer," *J. Fluid Mech.,* vol. 688, pp. 258-296, 2011.

[16] D. Huynh and B. McKeon, "Characterization of the Spatio-Temporal Repsonse of a Turbulent Boundary Layer to Dynamic Roughness," *Flow, Turbulence and Combustion,* vol. 104, pp. 293-316, 2019.

[17] S. Duvuuri and B. McKeon, "Triadic scale interactions in a turbulent boundary layer," *J. Fluid Mech.,* vol. 767, p. R4, 2015.

[18] N. Huthcins, T. B. Nickels, I. Mausic and M. S. Chong, "Hot-wire spatial resolution issues in wall-bounded turbulence," *J. Fluid Mech.,* vol. 635, pp. 103-136, 2009.

[19] F. O. Thomas, T. C. Corke, M. Iqbal, A. Kozlov and D. Shatzman, "Optimization of SDBD Plasma Actuators for Active Aerodynamic Flow Control," *AIAA Journal,* vol. 47, pp. 2169-2178, 2009.

[20] M. Wicks and F. O. Thomas, "Effect of Relative Humidity on Dielectic Barrier Discharge Plasma Actuator Body Force," *AIAA Journal,* vol. 53, 2015.

[21] M. Lozier, S. Midya, F. Thomas and S. Gordeyev, "Experimental Studies of Boundary Layer Dynamics Using Active Flow Control of Large-Scale Structures," in *TSPF-11*, Southhampton, UK, 2019.

[22] M. Lozier, F. Thomas and S. Gordeyev, "Streamwise Evolution of Turbulent Boundary Layer Response to Active Control Actuator," in *AIAA Scitech*, 2020.

[23] T. S. Luchik and W. G. Tiederman, "Timescale and structure of ejections and busts in turbulent channel flows," *J. Fluid Mech.,* vol. 174, pp. 529-552, 1987.

[24] H. Schlicting, Boundary Layer Theory, 9th ed., Springer, 2017.

[25] C. Liu, I. Gluzman, M. Lozier, F. Thomas, S. Gordeyev and D. Gayme, "Spatial input–output analysis of large-scale structures in actuated turbulent boundary layers," *AIAA Journal,* vol. 60, pp. 6313-6327, 20222.

[26] C. Zhang and S. I. Chernyshenko, "Quasisteady quasihomogeneous description of the scale interactions in near-wall turbulence," *Phys. Rev. Fluids,* 2016.